Applied Catalysis A, General 607 (2020) 117858

DOI 10.1016/j.apcata.2020.117858

# Restricting the growth of Pt nanoparticles through confinement in ordered nanoporous structures

Arnab Ghosh<sup>a</sup>, Hien Pham<sup>a</sup>, Jack Higgins<sup>a</sup>, Frank Van Swol<sup>a</sup>, Andrew DeLaRiva<sup>a</sup>, Matthew Melton<sup>a</sup>, Deepak Kunwar<sup>a</sup>, Gongshin Qi<sup>b</sup>, Se H. Oh<sup>b</sup>, Michelle Wiebenga<sup>b</sup>, Wei Li<sup>b</sup>, Abhaya K. Datye<sup>a,\*</sup>

<sup>a</sup>Department of Chemical & Biological Engineering and Center for Micro Engineered Materials, University of New Mexico, Albuquerque, NM 87131, USA

<sup>b</sup>General Motors Global Research and Development, Chemical and Materials Systems Lab, Warren, MI 48090, USA

\*datye@unm.edu

# **Keywords**

Diesel Oxidation Catalysts, Vapor Phase Transport, Accelerated Aging, Mesoporous Silica, Pore Confinement

#### Abstract

Accelerated aging of Pt diesel oxidation catalysts at 800 °C in the air causes vapor-phase emission of PtO<sub>2</sub> leading to severe deterioration in catalyst activity. Here we show that the growth of Pt nanoparticle size can be restricted by locating the Pt within nanosized pores. The mechanism of Pt sintering within the pores changes from vapor phase transport to surface diffusion because the pore volume is rapidly saturated with gas-phase PtO<sub>2</sub>. This causes Pt particle growth within the pores to be restricted. Knudsen diffusion helps to slow the rate of Pt emission compared to an open-pore silica gel. However, the PtO<sub>2</sub> that escapes from the pores grows to micron-sized particles, leading to loss of activity. The Pt retained in the pores grows large enough to block access to gas-phase reactants. These results provide insights for the design of pore structures to improve the durability of exhaust emission catalysts.

#### Introduction

Metal nanoparticle growth via Ostwald ripening is one of the major causes of catalyst deactivation [1]. The loss of active surface area due to the formation of large particles leads to loss of reactivity for surface catalyzed reactions [2]. The CLEERS Low-Temperature Oxidation Catalyst Test Protocol recommends an accelerated aging temperature of 800°C in 10% O<sub>2</sub> for 50 hrs to simulate the loss of performance of Pt DOCs after 150 k miles of driving [3]. During aging at 800°C, Pt sinters readily to form large particles [4]. At 800°C in the presence of oxygen, Pt forms volatile PtO<sub>2</sub> [5] and the high vapor pressure (1.6×10<sup>-8</sup> atm at 800°C) is responsible for vapor phase assisted ripening. Plessow et. al. [6] showed through DFT calculations that silica has negligible binding to PtO<sub>2</sub> suggesting that vapor phase transport dominates catalyst sintering. The role of vapor phase transport is adequately demonstrated via experiments involving physical mixtures of catalysts where Pt is transferred to neighboring particles. Carrillo et al. [7] showed on a model catalyst that Pt migrated to neighboring PdO particles within 2 minutes of heating at 650 °C in air. A longerrange transport of Pt was observed by Xiong et al. [8] when Pt migrated from Pt/MgAl<sub>2</sub>O<sub>4</sub> to physically mixed PdO/La-Al<sub>2</sub>O<sub>3</sub> at 800 °C in air, forming bimetallic Pt-Pd particles. The formation of anomalously large Pt particles was linked to the emission of volatile PtO<sub>2</sub> to the vapor phase [9]. The migration of Pt from wash coat monoliths in diesel oxidation catalysts (DOC) at 650 °C to downstream selective catalytic reduction (SCR) catalysts were shown to lead to ammonia oxidation and NOx formation in the exhaust [10] [11]. This Pt migration through the vapor phase is a serious challenge since it can lead to an increase in NOx tailpipe emission catalyst by as much as 3.6x from the NOx limit of 0.4 g/kWhr [11]. In related work, researchers at FORD showed that a loss of activity for the Pt and Pt-Pd catalysts could be directly related to the rate at which Pt was migrating downstream during high-temperature oxidative aging [12][13].

One approach to prevent the formation of large Pt particles is via the addition of Pd to these catalysts [14]. Since Pd and Pt are miscible and form alloys, this tends to lower the vapor pressure of Pt [15]. In a previous study [16], we examined the mechanisms that help slow Pt sintering and concluded that in addition to lowering of the vapor pressure, the trapping of volatile PtO<sub>2</sub> by PdO helps to restrict the growth of Pt particles. Another approach to slow down the sintering is by trapping the volatile species on reducible supports like ceria. Atom trapping was cited by Jones et. al. [17] as a mechanism for stopping the growth of Pt particles since physically mixing ceria with

Pt/La-Al<sub>2</sub>O<sub>3</sub> trapped all of the Pt onto the ceria support in the form of single atoms that were stable at 800°C in air. Work done by Shinjoh [18] demonstrates the stabilization of Pt by using a yttria-stabilized ceria-zirconia (CZY) under oxidizing conditions at 800°C in air since the author was able to stabilize the high-oxidation state of Pt. Kunwar et al. [9] demonstrated that the trapped Pt atoms on ceria have negligible vapor pressure, resulting in shutting down the emission of Pt to the vapor phase. Given the correlation between the transport of Pt to the vapor phase and the growth of large Pt particles and loss of catalyst activity, there is a need to explore other approaches to slow the emission of Pt in the form of volatile oxide to the vapor phase.

In their review article, Wynblatt and Gjostein [19] pointed out the importance of porous supports for achieving high dispersion of metal nanoparticles. These authors argued that metal particles on a convex surface will be less stable than those particles located on a concave surface, due to increased contact between the metal and support. It was also suggested that crystallites with dimensions similar to those of the pores are stabilized against sintering. Mesoporous supports are well-suited for investigation of the role of pore size (which is well defined), and the role of curvature (since the cylindrical pores have only concave surfaces). Liu et al. [20] stabilized subnanometric Pt in zeolites but their catalyst was calcined at 540°C, a temperature at which vapor phase transport was not the dominant sintering mechanism. The role of pore structure and connectivity has been studied in the context of the sintering of Au/SiO<sub>2</sub> [21]. It was found that even though the Au particles were initially located within the pores of mesoporous silica, after sintering the particles had grown in size breaking the pore walls. In another study of pore size effects, Lee at al. [22] found that bicontinuous pore structures allowed the Au to migrate outside the pores and form large particles. The 1-D pore structure of SBA-15 was more effective at maintaining Au within the pores, but the particle sizes had grown larger than the pore size based on the images presented in this work. In the absence of reactivity measurements, it is difficult to know if this strategy was successful to improve the catalytic activity. Catalytic measurements of pore-confined particles were presented by Prieto et al. [23] for methanol synthesis of Cu/ZnO-modified mesoporous silica. The Cu particles remained smaller than the pore size after reaction measurements conducted over 250 hours on stream. Work done on stabilizing Au nanoparticles at 800°C [24][25] and 550°C [26] have been reported by various groups but the vapor pressure of metallic Au is 1.69x10<sup>-11</sup> atm at these operating conditions which is too low to cause vapor phase transport. These previous studies

do suggest that mesoporous silica may be beneficial in controlling the growth of metal crystallites. However, none of these previous studies were performed under conditions where vapor-phase transport was responsible for catalyst sintering.

In this work, we explore whether pore confinement could help control particle size growth when vapor-phase dominates under the aging protocol used for diesel oxidation catalysts. We hypothesized that the vapor phase transport of Pt nanoparticles could be controlled by confining the Pt in mesopores since gas-solid equilibrium would be established almost instantaneously causing particle growth to cease, as shown schematically in Figure 1. We based this prediction on the rate of Pt evaporation in the air which is very rapid [27] and the vapor pressure of PtO<sub>2</sub> in contact with Pt metal [5], so a typical pore of SBA-15 which is 6 nm in diameter would require very few atoms of Pt to evaporate before equilibrium is established. This suggests that confinement of the nanoparticles within pores might help slow the transport of PtO<sub>2</sub> molecule through a porous network and ultimately the loss of Pt downstream from a DOC. Our goal was to understand the differences between an open pore silica gel and ordered 1-D mesoporous pore structures of MCM-41 and SBA-15. By aging powder samples in various geometries (thin film and packed bed), we were able to investigate the emission of Pt to the vapor phase and aging of larger samples allowed the performance of these aged Pt catalysts in CO oxidation to be determined. We found that while Pt can indeed be retained within the pores, and particle size controlled, access to the pore structure is lost as particles grow in size. This work provides clues for utilizing mesopore structures for improving the performance of Pt catalysts subjected to high-temperature aging.

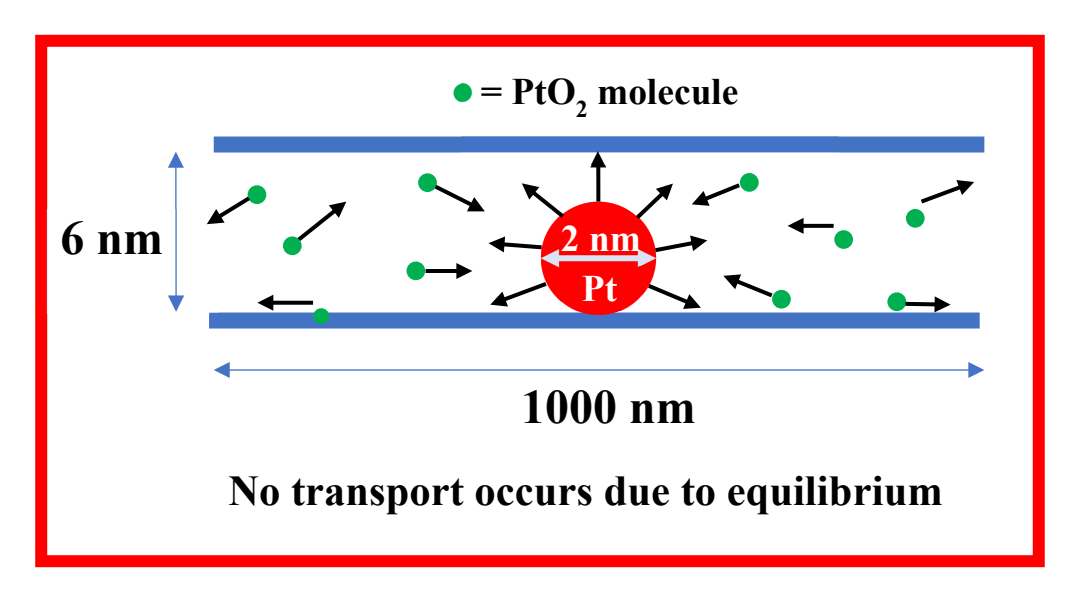
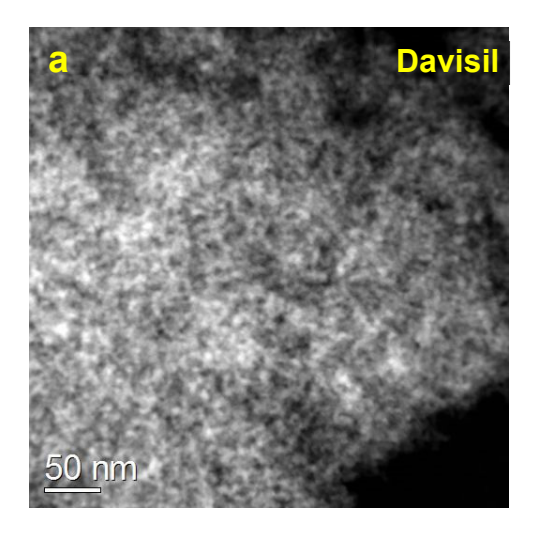


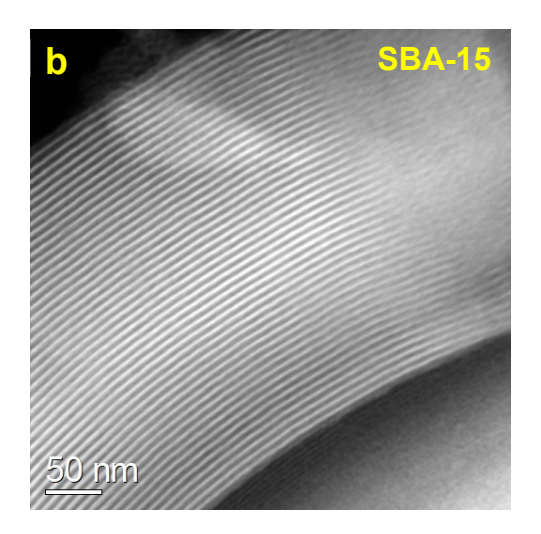
Figure 1. Schematic showing how establishing equilibrium inside a pore of SBA-15 can limit the transport of mobile PtO<sub>2</sub> species

# 2. Experimental

## 2.1 Catalyst preparation and aging

The Davisil silica gel (SiO<sub>2</sub>), mesoporous MCM-41 (SiO<sub>2</sub>), and the Chloroplatinic Acid (H<sub>2</sub>PtCl<sub>6</sub>) (precursor) were purchased from Sigma Aldrich. Mesoporous SBA-15 (SiO<sub>2</sub>) was prepared in the lab by a modified in-house recipe, 30 mL of DI water was taken along with 4g of Pluronic P123 which is a symmetric triblock copolymer, and stirred continuously with a magnetic stirrer until dissolved. The next step involved adding 120 mL of 2M Hydrochloric acid (HCL) along with 9.2 mL of Tetraethyl orthosilicate (TEOS). The solution was kept in a water bath for 24 hrs at 35°C, then the slurry was taken and filtered in a vacuum and the residue was collected and dried in a box furnace overnight to obtain the SBA-15. For this study, three different pore structures were studied as shown in Figure 2, Pt/Davisil (open pore structure, 15 nm average pore diameter), Pt/MCM-41, and Pt/SBA-15 (one-dimensional pore structure, 3 nm, and 6 nm pore diameters respectively).





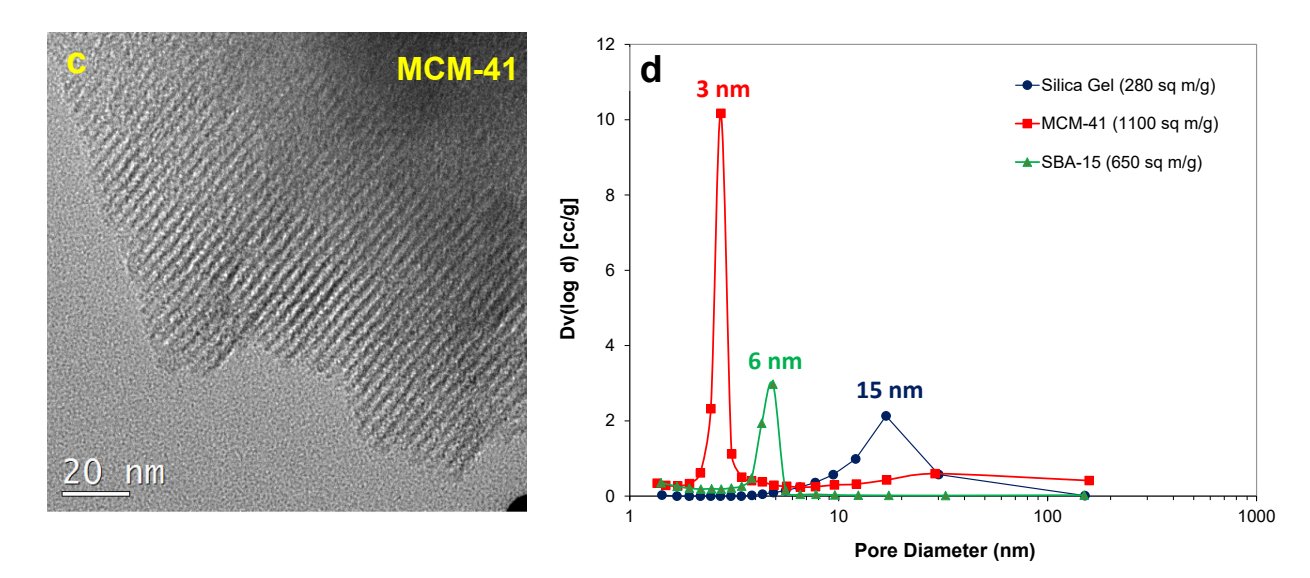


Figure 2. STEM Images of (a) Davisil (b) SBA-15 (c) MCM-41 showing the 1-D pore structure of the mesoporous silica and (d) Pore size distribution of Davisil (Silica Gel), MCM-41 and SBA-15

The Pt catalyst samples (supported on Pt/Davisil, Pt/SBA-15, Pt/MCM-41) were prepared by a wet impregnation process with an equivalent amount of 1.5wt% Pt with the supports and stirring them with 100 mL of De-ionized (DI) water then vacuum dry it at 40°C in a rotovap and scraping the powder off the glass wall. The powder was next loaded in a ceramic boat and placed in a tube furnace and treated in flowing H<sub>2</sub> at 200°C for 2 hrs at a slow ramp rate of 0.73°C/min to produce

the desired as-prepared catalyst. To visualize the internal pore structure, we created Pt nanowires inside the pores of SBA-15 by the wet reduction technique performed in flowing H<sub>2</sub> saturated with water vapor at 200°C for 2 hrs with a similar ramp rate of 0.73°C/min [28]. The experiments were performed in different sample test configurations that make it possible to study the vapor phase emission process as shown in Figure 3. When the sample is dispersed as a thin film on the wafer sample, there is minimal re-adsorption and the PtO<sub>2</sub> vapor can easily escape as it is swept away by the flowing air. Although the loss of Pt was observed when the sample was present in the form of a thin film (wafer geometry - Fig. 3a), no loss of Pt was observed by Scanning Electron Microscopy Energy Dispersive Spectroscopy (SEM-EDS), when we aged the same sample present in a ceramic crucible (boat geometry – Fig. 3b). This is because much of the Pt that was emitted to the vapor phase was re-adsorbed within the sample. This led to the formation of large Pt particles as we will show later. We also studied the catalyst in the form of a packed bed (Fig. 3c). At one extreme, we created a very thin packed bed to resemble the thin film we studied in the wafer geometry. The difference between the wafer geometry (Fig. 3a) and the shallow packed bed (Fig. 3c) is that the air flowed over the powder in the wafer geometry but through the bed in the case of the shallow packed bed. The mass transfer coefficient would be very different in these two cases, allowing us to determine how the rate of Pt emission is affected by the transport process.

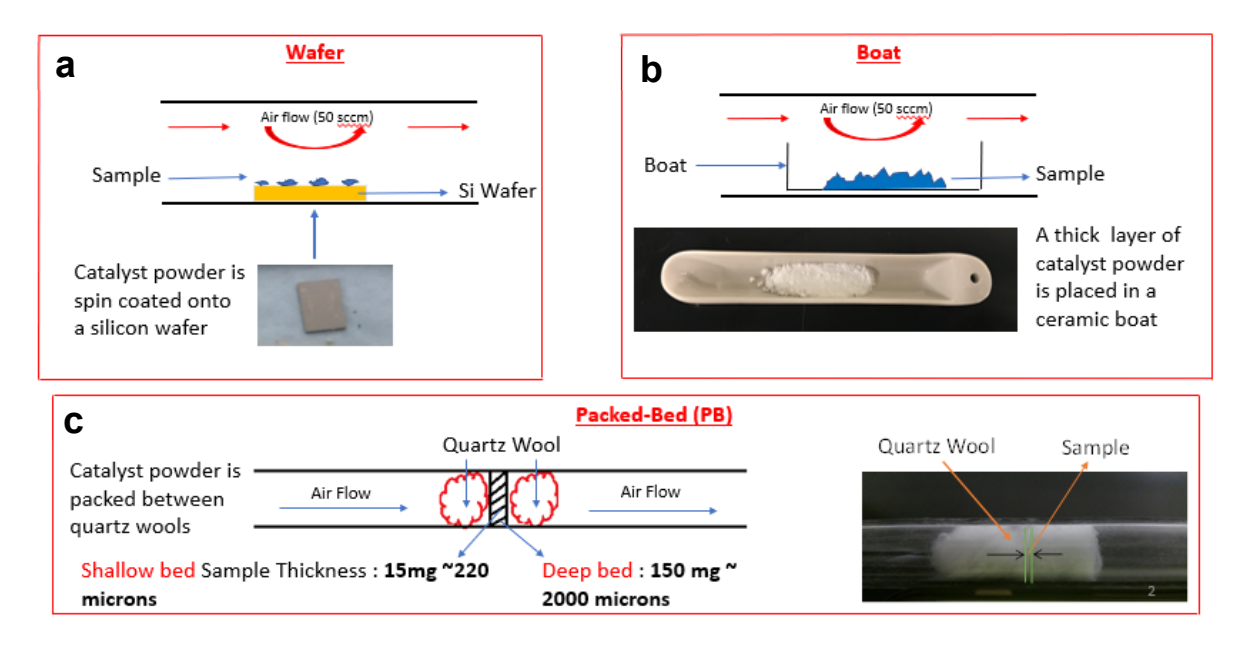


Figure 3. Configurations used for the study of Pt emission (a) The dispersed catalyst on a silicon wafer (Wafer Geometry), (b) The catalyst placed inside a ceramic boat (Boat Geometry) and (c) The catalyst as a packed bed in a thin layer of ~220 microns and packed between quartz wool (Thin packed Bed Geometry) or a thick layer of ~2000 microns (Deep Packed Bed Geometry).

A small amount of the as-prepared catalyst was dispersed in ethanol and mounted using a pipette on the silicon wafer and spin-coated as shown in Figure 3a, known as wafer geometry. The asprepared sample was placed in a ceramic crucible boat where 300 mg of the sample was used to make a deep bed as shown in Figure 3b which we have termed the boat geometry. The as-prepared sample was placed in between two quartz wool plugs in a flowing tube furnace where about 15 mg of the sample was used to cover the entire surface of the quartz wool creating the shallow packed-bed geometry shown in Figure 3c. In some experiments, we used a deep packed bed containing 150 mg of catalyst. These different types of aging configurations enabled us to detect the loss of Pt from the samples with varying diffusion distances to the flowing air. In a shallow bed, the air flows around the grains of the support while in a boat geometry the air flows over the top surface as shown in Figure 7. The treatment protocol involved heating the sample in a quartz tube at 800°C for 5 hrs in flowing air at 50 sccm.

## 2.2 Catalyst Characterization

After aging the powder catalysts using the different configurations at 800°C for 5 hrs in flowing air we determined the content of Pt using SEM-EDS. The Si wafer with the dispersed catalyst on it (Figure 3a) was placed on a double-sticky carbon tape and transferred to an aluminum SEM stub. A typical region analyzed is shown in Figure 4. The carbon tape allowed EDS analysis without interference from the underlying Al stub. A total of 15 such regions (field of view 250 μm x 250 μm) were analyzed by SEM-EDS at 15 kV. The average of

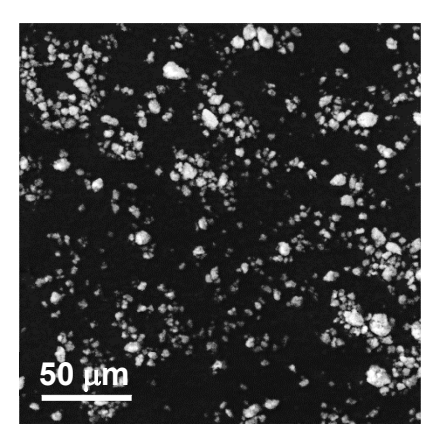


Figure 4. Typical region analyzed in the SEM for each EDS spectrum. The sample shown is Pt/Davisil-1.5wt%Pt

these regions was reported as a Pt wt% for the as-prepared and aged samples. SEM-EDS was used since it provides a better average and larger grains can be studied compared to TEM-EDS where smaller regions of the sample can be studied. The experimental error was derived from the confidence interval based on the t-distribution of the EDS data. While the sample is uniform in the as-prepared state, there is inherent heterogeneity in the sample after aging. This is reflected in the larger error bars for the data on the aged samples. Bulk elemental analysis was performed using Inductively Coupled Plasma - Optical Emission Spectrometry (ICP-OES) which could only be used with the deep bed samples since we need at least ~50 mg of the sample to gain the necessary accuracy for determining Pt content. This analysis was done by Galbraith laboratories and the reported error by the lab was about  $\pm 10\%$  which is comparable with the confidence interval from EDS analysis. Transmission electron microscopy (TEM) was performed at 200 kV using a JEOL 2010 Field Emission Gun (FEG) TEM/STEM equipped with an Oxford energy dispersive X-ray spectroscopy (EDS) system. The catalyst was ground with a mortar and pestle and dispersed in ethanol. A drop of this suspension was deposited on TEM copper grids containing a holey carbon film. A Micromeritics ASAP 2020 was employed to determine the N<sub>2</sub> adsorption isotherms and the resulting BET surface area for each sample.

## 2.3 Reactivity Measurements

CO oxidation was chosen as a probe reaction. The activity of the unaged and aged samples was measured with 20 mg of the sample placed inside a ¼ inch diameter U-tube stainless-steel reactor which was heated in a programmable temperature convection oven. The gas flow rates for CO oxidation were: CO 1.5 ml/min, O<sub>2</sub> 1 ml/min, and He 75 ml/min, and the temperature ramp rate was at 2°C/min.

# 2.4 Molecular Dynamics Computations

To understand the competing effects of pore diameter and pore length, we performed molecular dynamics simulations of  $PtO_2$  molecules. We represented this molecular species as a single atom. Given that the transport of  $PtO_2$  takes place in the low-density Knudsen diffusion regime, we focused entirely on the interaction between the transporting atom and the wall, ignoring all other interatomic interactions. Our system consisted of a collection of independent ideal gas atoms diffusing out of a smooth cylindrical pore. We describe the interaction between the atom and the wall by a (truncated and shifted) 12-6 Lennard-Jones (LJ) potential. Each atom is released from a position half-way the pore length and at the radial center of the pore. To account for the Maxwell distribution of velocities, we assign an initial velocity vector that is randomly selected from a normal distribution. The dynamical trajectory is obtained by time-stepping, using the Verlet algorithm. The primary effect of the dynamic wall atoms is to turn the wall 'collision' into a non-specular inelastic collision, we decided to capture this effect by using Langevin dynamics for atoms close to the wall, i.e., within the attractive LJ well. Conveniently, Langevin dynamics has a single (diffusion) parameter ( $\gamma$ ), that characterizes its diffusive nature near the wall. Also, for  $\gamma$ =1 Langevin dynamics reduces to standard Newtonian dynamics.

## 3. Results and Discussion

## 3.1 Stability of the supports

The BET surface areas for the Davisil, SBA-15, and MCM-41 bare supports and Pt catalyst samples, before and after the 800°C for 5 hrs treatment are reported in Table 1. As seen from this Table, the nanoporous supports are thermally stable and suffer minimal loss in surface area after 800°C aging, except for SBA-15 which loses micro-porosity in the walls, which causes a

decrease in BET surface area. The significant decrease in the BET surface area of the Pt/silica catalysts after aging is a result of the growth of Pt particles and possible pore blockage, which is most severe in the case of the MCM-41 support. This is also confirmed by the loss in pore volume (Figure S1).

Table 1. BET Surface Areas of the catalysts used in the study

Support	Catalyst Support		1.5 wt% Pt/silica (m²/g)	
	$(m^2/g)$			
	As prepared	After aging at 800°C for 5hrs	As prepared catalyst	After aging at 800°C for 5hrs
Davisil	287	272	276	76
SBA-15	607	320	475	39
MCM-41	1098	1040	830	14

# 3.2 Emission of Pt to the vapor phase in the wafer geometry

Experiments using a thin film of catalyst (wafer geometry – Fig. 3a) were performed to make it easy to detect Pt loss from the catalyst. In this approach, the individual grains of the catalysts are exposed to the vapor phase and there is a minimal chance of re-adsorption of the mobile PtO<sub>2</sub>. The as-prepared samples were found to contain ~1.5wt% Pt via SEM-EDS which is close to the nominal loading. Five different samples were prepared for each of the catalysts, Pt/Davisil, Pt/SBA-15, and Pt/MCM-41 and they were monitored at 1 hr intervals for a total of 5 hrs. In this manner, the role of pore size on Pt emission could be studied. We found out via SEM-EDS that Pt/Davisil lost the most (~67% of the original Pt was lost) since it has an open pore structure with larger pores (15 nm) compared to the Pt/SBA-15 (6 nm pores) and Pt/MCM-41 (3 nm pores) which lost (~40% and ~49% respectively). As we expected, the one-dimensional pores tend to slow the rate of Pt loss to the vapor phase as seen in Figure 5. The loss of Pt is also consistent with the work of Kunwar et. al. [9] where they observed a complete loss of Pt under similar conditions in 7 hrs at 800°C for both Pt/La-Al<sub>2</sub>O<sub>3</sub> and Pt/MgAl<sub>2</sub>O<sub>4</sub>.

We see a linear decrease in Pt content as a function of time for all of the catalysts as shown in Figure 5. The lack of dependence on the amount of Pt left behind on the sample suggests that the slow step in Pt loss is the intrapore diffusion of PtO<sub>2</sub> vapor. The differences in the rate of loss

from the three supports further indicate that this is a transport limited process. To our surprise, we found out that Pt/MCM-41 lost more Pt than the Pt/SBA-15 although MCM-41 has 3nm diameter pores compared to 6nm pores for SBA-15. As we show later, the pore length of MCM-41 was much shorter than that of SBA-15, which explains the observed effect on the rate of Pt loss.

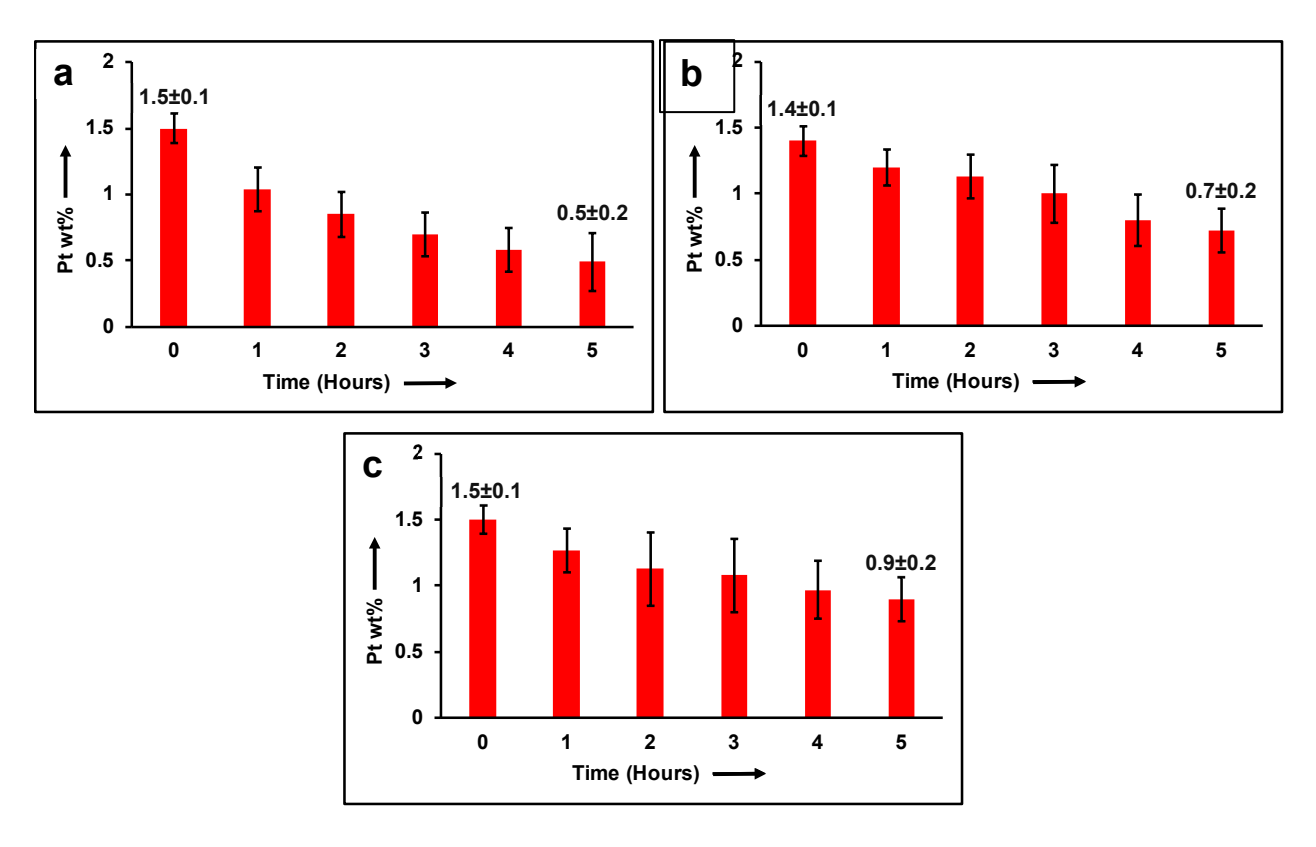


Figure 5. Aging using the wafer geometry at 800°C for 5 hrs in air flowing at 50 sccm (a) 67% of Pt was lost from 1.5wt% Pt/Davisil (b) 49% of Pt was lost from 1.5wt% Pt/MCM-41 (c) 40% of Pt was lost from 1.5wt% Pt/SBA-15

## 3.3 Emission of Pt to the vapor phase in the shallow packed-bed geometry

To study the role of external mass transfer, we studied the configuration shown in Figure 3c where the gas flows through a bed. This is in contrast to the geometry studied in Figure 3a where a similar thin layer was used but the gas flows over the catalyst rather than through the bed. We made the catalyst bed extremely thin (15 mg of the catalyst which translates to a catalyst depth of ~200 microns) to achieve the same sensitivity to Pt loss. This allowed us to make measurements similar to that of the wafer (Figure 3a) by exposing the powder to the aging protocol while minimizing a chance for re-adsorption of the Pt. The amount of Pt that was lost on the wafer geometry and the shallow packed-bed geometry was very similar although the external diffusion distances were

radically different (Figure 6). The external diffusion distances for PtO<sub>2</sub> in the shallow packed bed are orders of magnitude smaller (~nm) as compared to (~mm) on the wafer shown in Figure 7. Since a smaller diffusion length translates into a higher rate of mass transfer, we would have expected to see a greater amount of Pt lost from the shallow packed bed as compared to the wafer.

The content of Pt in the catalyst before and after aging was determined using SEM-EDS and the sample was aged at 800°C for 5 hrs under flowing air of 50 sccm. From our SEM-EDS results shown in Figure 6 we found out that Pt/Davisil lost the most amount of Pt (~64% of the initial Pt loading was lost) followed by Pt/MCM-41 (~48% of the initial Pt loading was lost) and Pt/SBA-15 lost the least amount of Pt (~38% of the initial Pt loading was lost). The rate of mass transfer of volatile species of PtO<sub>2</sub> is therefore determined by the internal pore structure. We conclude that the rate-limiting step must be the intraparticle transport of the PtO<sub>2</sub> mobile species from inside the pores to the gas phase, and the nanopore structure plays a significant role.

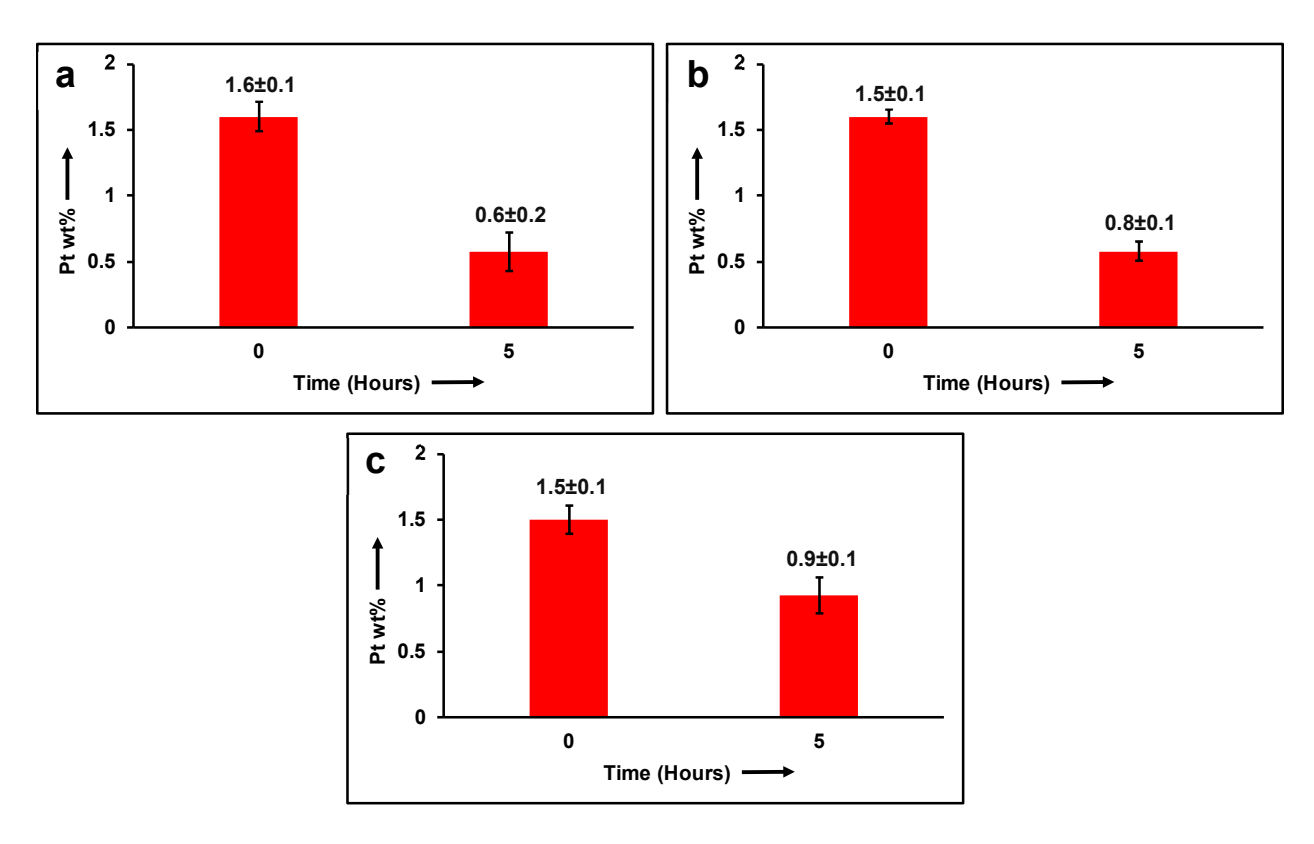


Figure 6. Aging using the thin packed bed configuration at 800C for 5 hrs in flowing air at 50 sccm (a) 64% of Pt was lost from 1.5wt% Pt/Davisil (b) 48% of Pt was lost from 1.5wt% Pt/MCM-41 (c) 38% of Pt was lost from 1.5wt% Pt/SBA-15

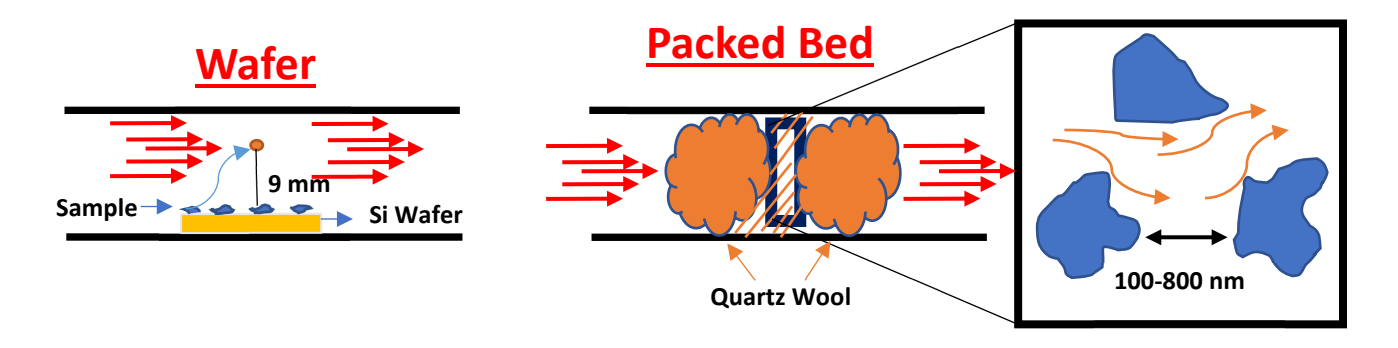


Figure 7. Diffusion length for PtO<sub>2</sub> in the wafer geometry and shallow packed-bed geometry.

#### 3.4 Influence of pore size on PtO<sub>2</sub> emission to the vapor phase

The transport of PtO<sub>2</sub> from 3 nm diameter pores would be expected to be slower compared to the 6nm diameter pores. But we observed exactly the opposite, the 6 nm pores lost less Pt than the 3 nm over the same duration of catalyst aging. On closer inspection of the pore structure, we realized that the pore lengths of the two mesoporous silicas are quite different. We performed SEM Imaging (Figure S2) and found out that the average size of the particles of SBA-15 and MCM-41 are 553nm and 191nm respectively, which we would expect to be the length of the pores inside these particles. However, the SEM images do not reveal the internal pore structure, for instance, if there is overlap in pores within the 3D structure. Therefore, we used the wet reduction technique described in the experimental section according to Bore et. al [28] to create nanowires of Pt inside SBA-15. This allowed us to map the internal pore network of the mesoporous silica, as shown in Figure 8a. The STEM image shows us how the pores fold over each other and the effective length of the pores is roughly around ~1 micron rather than the 553 nm we estimated based on the SEM images. This knowledge of the pore network lengths of the mesoporous silica helps in understanding the emission rates of PtO<sub>2</sub> from these silica samples.

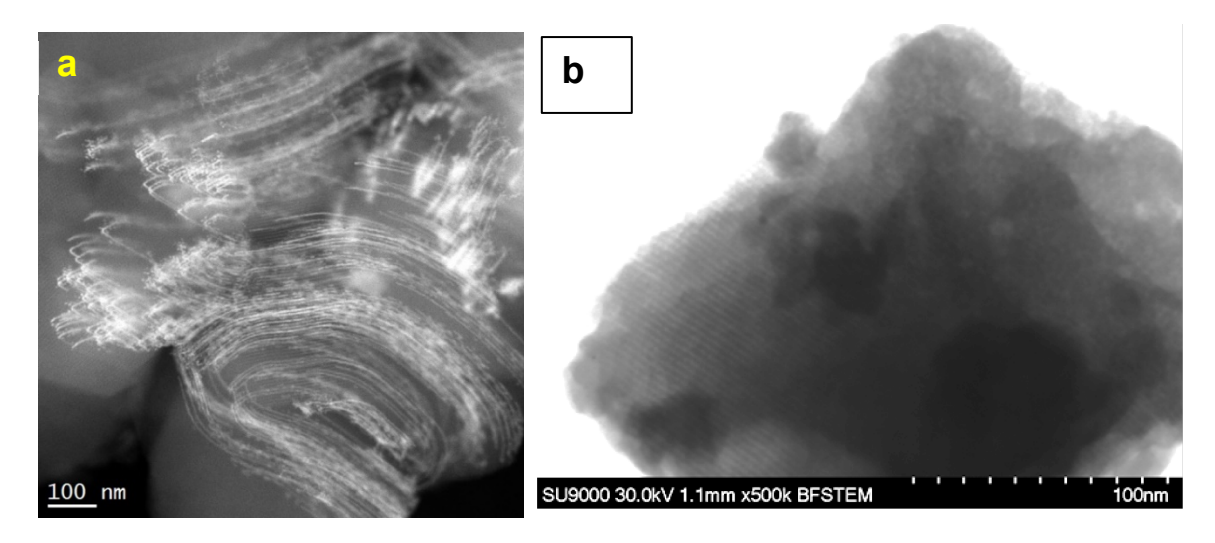


Figure 8. (a) STEM Image of SBA-15 showing the pores fold over doubling their effective length to ~1 micron, as compared to (b) Pores in MCM-41 do not fold over, yielding an average pore length of 191 nm based on the size of the particles.

Molecular Dynamics (MD) simulations were performed as described earlier in section 2.4 to understand the competing effects of pore diameter and pore length on Pt emission characteristics. Cumulative Distribution Functions (CDF) showing the fraction of Pt that is emitted from within the pore structure as a function of LJ time as are shown in Figure 9. For this simulation, the SBA-15 support was taken to be the base case (6 nm pore diameter) and the pore length was varied from 25 nm to 100 nm. From Figure 9, after 200 MD cycles, the 25 nm pore length lost ~98% of the Pt, 50 nm pore length lost ~80% of the Pt, and the 100 nm pore length lost ~40%. Using a similar approach, we also performed MD simulations for an 80 nm long pore with pore diameters of 3 nm and 6 nm (MCM-41 and SBA-15) (Figure 9b). After 200 MD cycles, the Pt lost was 38% and 55% for the 3 nm and 6 nm pore diameters, respectively. However, with longer pores, the 6 nm sample lost only 40% (Figure 9a). These MD simulations suggest that longer pores could have reduced the loss from SBA-15 to a level similar to MCM-41. Since the ratio of pore lengths between SBA-15 and MCM-41 ~5:1, we can understand why SBA-15, despite its larger diameter pores, loses less Pt.

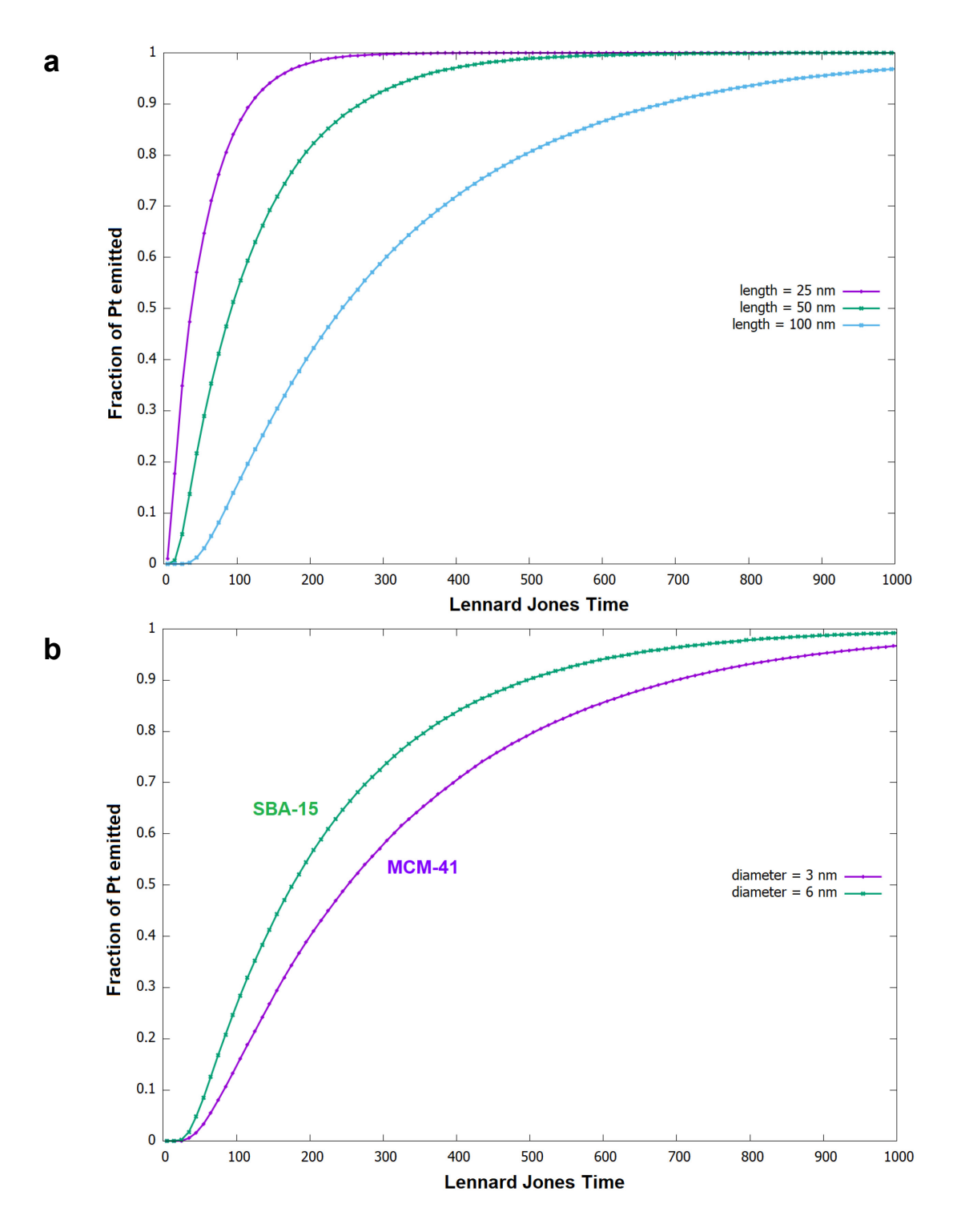


Figure 9. The total number of simulated molecules is 100,000 PtO<sub>2</sub> at T=800°C a.) MD Simulation for exit time of PtO<sub>2</sub> emitted from a 6 nm SBA-15 pore of varying pore lengths ranging from 25 nm to 100 nm show a dependence in PtO<sub>2</sub> emission as a function of pore length.

b.) MD Simulation for exit time of PtO<sub>2</sub> emitted from SBA-15 and MCM-41 from a 80 nm pore length.

# 3.5 Emission of Pt to the vapor phase from the deep packed bed

To resemble more closely the architecture of a catalytic converter in a vehicle, we measured the Pt emission from the surface of a deep bed (Figure 3c). The amount of catalyst used was ~150mg (equivalent catalyst depth of ~2000 microns). By using a larger amount of the catalyst, we were able to perform bulk elemental analysis via Inductively Coupled Plasma - Optical Emission Spectroscopy (ICP-OES). This allows for reliable quantification of the amount of Pt lost from the bed, and it allows us to study the effect of the flow rate of air on the emission of Pt from a deep bed sample. The aging was done on Pt/Davisil and Pt/SBA-15 in a ceramic crucible boat containing respectively 1.2 and 1.5 wt% of Pt. The samples (4 aliquots of each support), were aged at 800°C for 5 hrs using flow rates of 5, 25, 75, and 100 sccm as shown in Table 3.

Table 3. ICP-OES showing Pt content after aging, as a function of flow rate

Flow Rate (sccm)	Davisil	SBA-15
5	1.08	1.59
25	1.12	1.63
75	1.06	1.61
100	1.02	1.57

**Note:** Galbraith laboratories reported an error of  $\pm 10\%$  for each ICP-OES measurement.

The ICP-OES data shows no change (within experimental error) in the Pt wt% when the air-flow rate was changed from 5 sccm to 100 sccm. This result is consistent with our observation that there is no effect on the rate of loss of Pt due to external mass transport. The rate-limiting step must be intrapore transport which is unaffected by changing the flow of air in the tube. This was evident also from the similar loss of Pt when we caused the air to flow through the grains of the catalyst (thin-bed Figure 3b) and over the grains (thin wafer Figure 3a).

# 3.4 Emission of Pt to the vapor phase from the crucible

We wanted to obtain more accurate measurements of Pt loss from a packed bed and also to age larger sample sizes so we could perform particle size measurements and study the reactivity of these catalysts for CO oxidation. For these experiments, we used 300 mg of powder placed in a ceramic crucible for aging. The as-prepared samples contained ~1.5wt% Pt nominal weight loading and were aged at 800°C for 5 hrs with 50 sccm of flowing air. Both the as-prepared and aged samples were analyzed by ICP-OES and no loss of Pt was reported, indicative of the fact that all the Pt that was emitted to the vapor phase emission was now re-adsorbed within the sample forming the large particles shown in Figure 10.

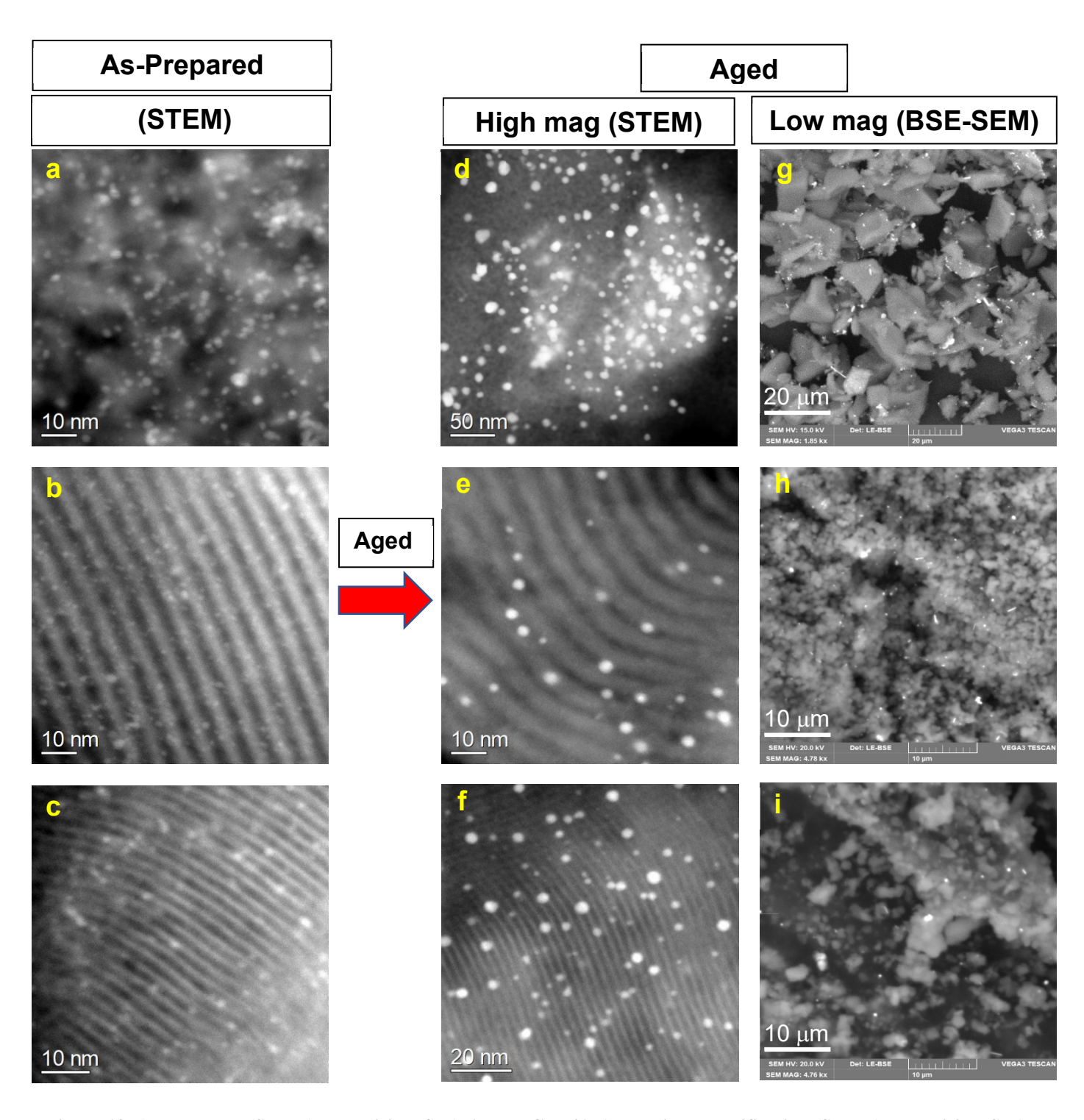


Figure 10. As-Prepared (STEM) a. Davisil b. SBA-15 c. MCM-41, Aged High magnification (STEM) d. Davisil e. SBA-15 f. MCM-41, Aged Low magnification (BSE-SEM) g. Davisil h. SBA-15 i. MCM-41.

These are the representative images of the samples and >200 particles were counted to derive the average particle size before and after the aging treatment. The Particle Size Distribution (PSD) for Pt/Davisil, Pt/SBA-15, and Pt/MCM-41 is provided in Figures S4-S6 which shows the average Pt particle size is ~2 nm for the as-prepared samples. In the initial sample, there was some sparse Pt cluster formation on the Pt/Davisil due to the similar charge of the precursor and the support but these clusters were not observed on the Pt/SBA-15 and Pt/MCM-41 because of the spatially distributed well defined porous nature of the supports. The STEM images show that the particles are uniformly dispersed throughout the sample and situated within the mesopores of the supports. After the aging treatment, the particle size became bimodal with particles ranging in size from nanometers to micron size particles. Due to the bimodal size distribution, we need to use both STEM and SEM to obtain better statistics since otherwise, any one technique would skew the average to large or small particles, respectively. Therefore, STEM was used to measure the particles that remained within the porous structure while SEM was used to measure the large particles.

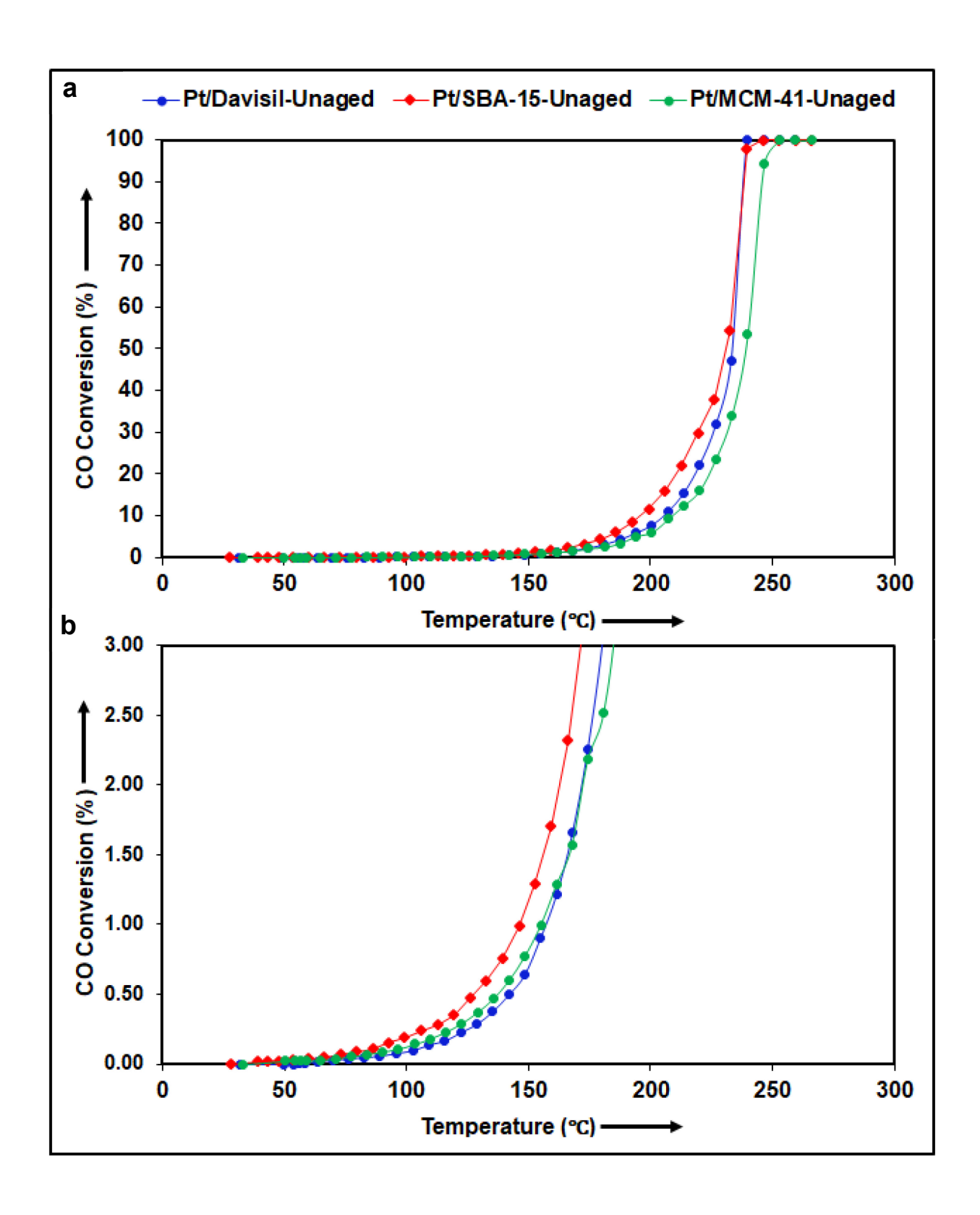
Table 2 shows that the particles counted using STEM images (Pt particles that remained within the pores after aging) on the Pt/Davisil, Pt/SBA-15, and Pt/MCM-41 supports have average particle sizes of 9.4, 5, and 3.4 nm. This implies that the mesoporous nature of these supports (SBA-15 and MCM-41) was able to limit the growth of Pt particle size to the respective pore sizes while the Davisil support with open pores yielded much larger Pt particles.

Table 3. Particle Size of Pt nanoparticles across different supports (the aged sample lists data in two columns because of the bimodal nature of the particle size distribution)

Support	Pore Size of Supports (nm)	As-prepared Pt Particle Size (STEM) nm	Aging at 800°C for 5hrs Pt Particle Size (STEM) nm	Aging at 800°C for 5hrs Particle Size (BSE-SEM) µm
Davisil	15 (Open Pore)	2.4	9.4	2.4
SBA-15	6 (1D Pore)	2	5	0.84
MCM-41	3 (1D Pore)	2	3.4	0.84

# 3.4 CO oxidation reactivity of the Pt catalysts

We also performed CO oxidation activity measurements to determine the performance of the catalysts before and after the aging treatment. Three runs of CO oxidation were performed for each sample, and the third run is reported in Figure 11 for both the initial and aged catalyst. Initially, the as-prepared catalysts have similar reactivity indicating that there are no mass transfer limitations despite the mesoporous structures of the supports. After aging, the reactivity of the catalysts decreases in the order of Pt/Davisil>Pt/SBA-15>Pt/MCM-41.



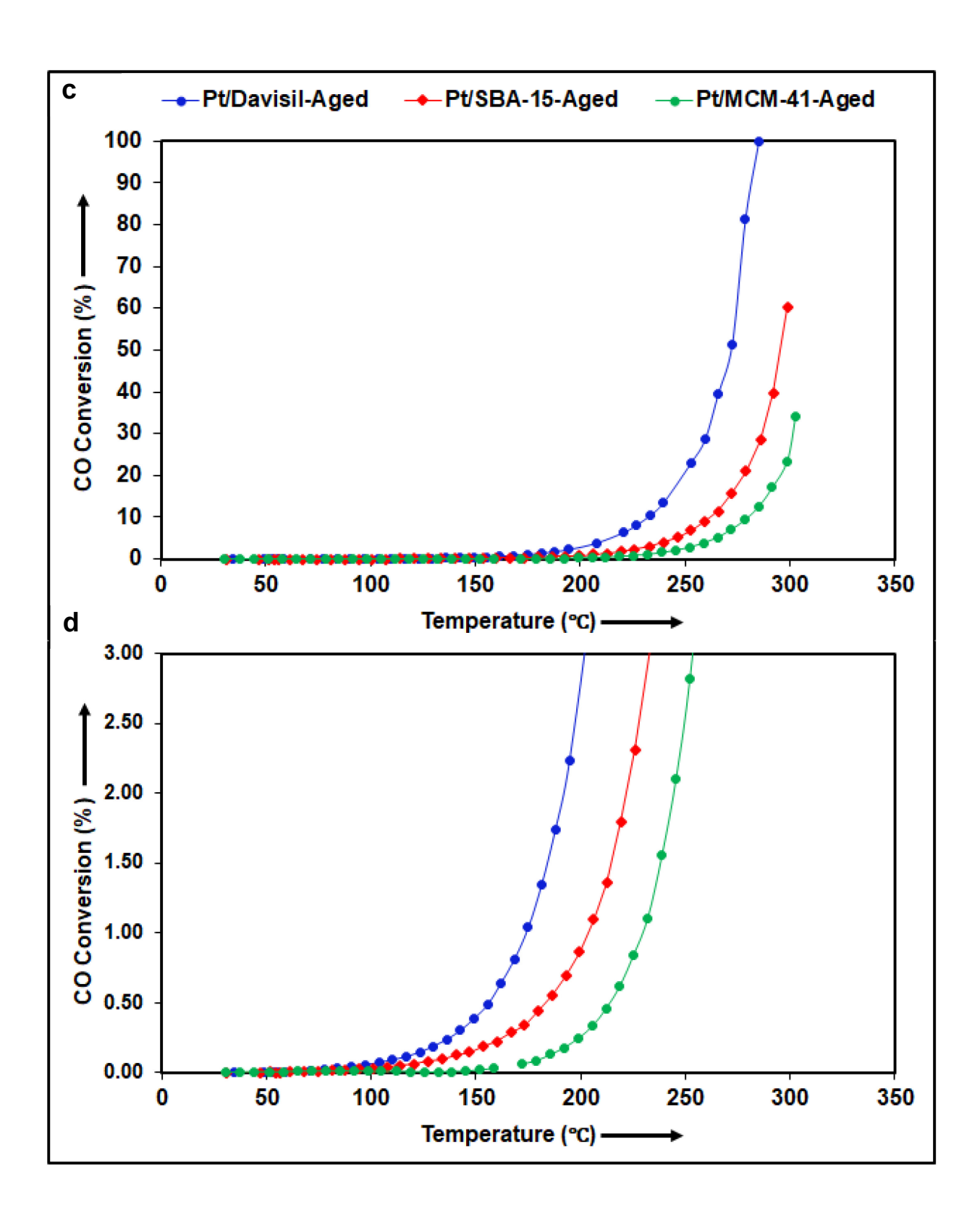


Figure 11. Light-off measurements for CO oxidation Unaged (a) from 0-100% CO conversion and (b) from 0-3% CO conversion. Light-off measurements for CO oxidation are also reported for Aged catalyst at 800°C for 5hrs in a crucible in air (c) from 0-100% CO conversion and (d) from 0-3% CO conversion. Temperatures were ramped at 2°C/min from 25°C to 300°C.

This was surprising since the Pt/MCM-41 sample had retained the smallest Pt particles inside the pores while the particles in Pt/Davisil had grown to over twice the size. The growth of Pt particles to a size comparable to the pore diameter or greater than the pore diameter (by breaking the pore walls in some cases), causes complete blockage of the pore and it is no longer a case of simultaneous pore diffusion and reaction. The catalytically active Pt in the sintered catalyst is located exclusively outside the mesopores as large particles and the small particles left behind in the mesopores are rendered completely inactive because they are inaccessible to the gas phase. This was confirmed by the N<sub>2</sub> adsorption measurements (Figure S1), the BET surface area, and the PSD after aging. A schematic showing the pore blockage by Pt particles after aging is shown in Figure 12.

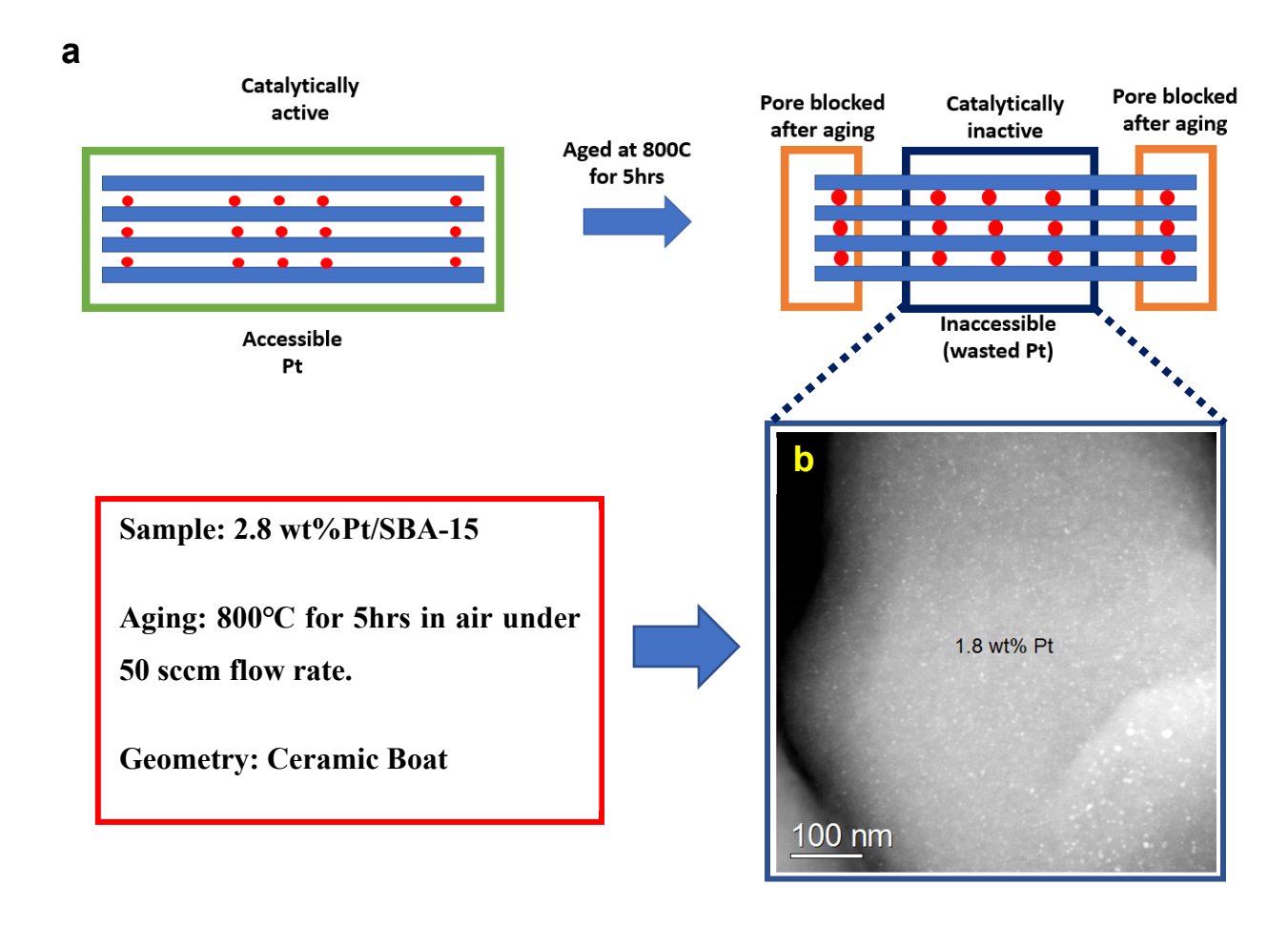


Figure 12. (a) Schematic showing pores accessible before aging and plugged after aging in the mesoporous supports. (b) Inset showing STEM image of 2.8 wt%Pt/SBA-15 after aging at 800°C for 5hrs in a crucible boat of which 1.8wt%Pt is confined within the pores while 1wt% came out of the pores and formed large Pt particles.

To estimate the fraction of Pt retained in the pores, we aged 2.8 wt%Pt/SBA-15 at 800°C for 5hrs in a crucible boat in the air and examined it via STEM as shown in Figure 12b. The amount of Pt that remained in the pores trapped and catalytically inactive was ~1.8 wt% Pt indicating that only ~1 wt% Pt was able to escape from the pores forming anomalously large particles. This explains why Pt/SBA-15 performed much worse than the open pore Davisil silica gel. Since the majority of the surface area in the mesoporous sample is inaccessible, the Pt outside the pores grows to larger particle sizes and less than 35% is available for reaction. Likewise, Pt/MCM-41 performs the worst because of smaller pores than the other two catalysts. The smaller pore size in MCM-41 causes extensive pore blockage to happen, leading to the counterintuitive result that the MCM-41

catalyst has the lowest reactivity. This is in agreement with the work done by Dhillon et al. [29] where they showed that reduction of pore size due to the formation of Al(OH)<sub>3</sub> layers in the wash coat had a detrimental effect on the activity of the catalyst. We would also expect a decrease in apparent activation energy due to transport limitations [30], but we do not see this because all of the active Pt in our catalyst is outside the pores. Our strategy of pore confinement was successful in limiting the growth of Pt particles that remained within the pores, but not in achieving higher reactivity. On the other hand, in a previous study [23] on the role of pore confinement for methanol synthesis, the Cu particles did not grow to the size of the pores and therefore did not impede the reactivity. Hence these authors [23] found a beneficial effect of using mesoporous silica.

# 3.5 Factors controlling the emission of Pt from the catalyst

All measurements were performed by heating the sample at 800°C for 5 hours, conditions where volatile PtO<sub>2</sub> formation leads to rapid loss of Pt to the vapor phase from the catalyst surface [27]. To properly quantify Pt loss, the Pt catalyst was deposited as a thin film on a Si wafer and then subjected to aging. Our results show that the amount of Pt loss decreased in the order of Pt/Davisil > Pt/MCM-41 > Pt/SBA-15. Based on MD simulations, we infer that both the diameter of the pore and its length would both influence the loss of Pt. Pt/MCM-41 exhibits a larger loss of Pt despite its smaller pore size because the pore length is 1/5th as long as that of SBA-15. These results demonstrate that confinement of Pt within nanoporous silica helps to slow the rate of Pt loss to the vapor phase and to control the growth of Pt particle size.

The primary resistance to Pt transport lies within the pores. In a packed bed, we found that changing the external airflow caused no change in the detectable loss of Pt by ICP-OES. By performing the measurements with the catalyst as a thin film and a shallow packed bed, we observed similar loss of Pt despite different diffusion lengths. This observation confirms that intraparticle transport limits the rate of Pt loss to the vapor phase.

The amount of Pt lost is below detection limits when we performed measurements using the catalyst powder placed in a crucible as a deep packed bed (~150 mg). This is because most of the Pt that was emitted to the vapor phase was re-deposited within the catalyst bed, leading to the formation of anomalously large Pt particles. Only a small amount of Pt was lost from the catalyst

surface to the vapor phase. However, this small loss of Pt from working DOC catalysts has a negative impact on downstream SCR catalysts [10 - 13].

#### **Conclusions**

The results presented here show that nanoporous supports can limit the growth of Pt particle size during aging at 800 °C in air, but only for the Pt present within the pores. Pore confinement was successful since vapor phase transport within the pores ceased once the gas phase reached saturation. This led to lower rates of emission of Pt to the vapor phase from the nanoporous silica supports. With regard to pore confinement, smaller diameter pores in MCM-41 were more effective at retaining smaller Pt particles than the larger diameter pores in SBA-15. However, in both of these supports, when the Pt particles grew to be equal or greater than the pore diameter, they blocked the transport of the reactants CO and O<sub>2</sub> to the active sites. The result was that after aging, the open-pore silica gel performed better for CO oxidation than the ordered nanoporous silica. The Pt that escaped from the pore mouths formed anomalously large particles, as large as microns in size, due to limited nucleation sites for the Pt. These results provide clues for the design of pore structures to improve the durability of Pt during lean accelerated diesel catalyst aging.

# Acknowledgments

Financial support from NSF GOALI grant CBET 1707127 and General Motors Global R&D. We thank the Earth and Planetary Sciences Department and Center for Micro Engineered Materials for use of characterization facilities and Hitachi for access to the SU-9000 high-resolution SEM/STEM for some of the images presented here.

## **References:**

- [1] T.K. Hansen, M. Høj, B.B. Hansen, T.V.W. Janssens, A.D. Jensen, Top. Catal. 60 (2017) 1333–1344.
- [2] G.W. Graham, H.W. Jen, O. Ezekoye, R.J. Kudla, W. Chun, X.Q. Pan, R.W. McCabe, Catal. Letters 116 (2007) 1–8.
- [3] T.J. Toops, V.Y. Prikhodko, J.A. Pihl, in: Emiss. Control Sci. Technol., Springer

- International Publishing, 2018, p. 135.
- [4] T.R. Johns, R.S. Goeke, V. Ashbacher, P.C. Thüne, J.W. Niemantsverdriet, B. Kiefer, C.H. Kim, M.P. Balogh, A.K. Datye, J. Catal. 328 (2015) 151–164.
- [5] C.B. Alcock, G.W. Hooper, Proc. R. Soc. London. Ser. A. Math. Phys. Sci. 254 (1960) 551–561.
- [6] P.N. Plessow, F. Abild-Pedersen, ACS Catal. 6 (2016) 7098–7108.
- [7] C. Carrillo, T.R. Johns, H. Xiong, A. Delariva, S.R. Challa, R.S. Goeke, K. Artyushkova,
   W. Li, C.H. Kim, A.K. Datye, J. Phys. Chem. Lett. 5 (2014) 2089–2093.
- [8] H. Xiong, E. Peterson, G. Qi, A.K. Datye, Catal. Today 272 (2016) 80–86.
- [9] D. Kunwar, C. Carrillo, H. Xiong, E. Peterson, A. DeLaRiva, A. Ghosh, G. Qi, M. Yang,M. Wiebenga, S. Oh, W. Li, A.K. Datye, Appl. Catal. B Environ. 266 (2020) 118598.
- [10] K. Leistner, C. Gonzalez Braga, A. Kumar, K. Kamasamudram, L. Olsson, Appl. Catal. B Environ. 241 (2019) 338–350.
- [11] E. Hruby, S. Huang, R. Duddukuri, D. Dou, SAE Tech. Pap. 2019-April (2019) 1–12.
- [12] H.W. Jen, J.W. Girard, G. Cavataio, M.J. Jagner, SAE Int. J. Fuels Lubr. 1 (2009) 1553–1559.
- [13] G. Cavataio, H.W. Jen, J.W. Girard, D. Dobson, J.R. Warner, C.K. Lambert, SAE Int. J. Fuels Lubr. 2 (2009) 204–216.
- [14] A. Morlang, U. Neuhausen, K. V. Klementiev, F.W. Schütze, G. Miehe, H. Fuess, E.S. Lox, Appl. Catal. B Environ. 60 (2005) 191–199.
- [15] J.B. Darby, K.M. Myles, Metall. Trans. 3 (1972) 653–657.
- [16] C. Carrillo, A. DeLaRiva, H. Xiong, E.J. Peterson, M.N. Spilde, D. Kunwar, R.S. Goeke,

- M. Wiebenga, S.H. Oh, G. Qi, S.R. Challa, A.K. Datye, Appl. Catal. B Environ. 218 (2017) 581–590.
- [17] J. Jones, H. Xiong, A.T. DeLaRiva, E.J. Peterson, H. Pham, S.R. Challa, G. Qi, S. Oh, M.H. Wiebenga, X.I.P. Hernández, Y. Wang, A.K. Datye, Science 353 (2016) 150–154.
- [18] H. Shinjoh, Catal. Surv. from Asia 13 (2009) 184–190.
- [19] P. Wynblatt, N.A. Gjostein, Prog. Solid State Chem. 9 (1975) 21–58.
- [20] L. Liu, U. Díaz, R. Arenal, G. Agostini, P. Concepción, A. Corma, Nat. Mater. 16 (2017) 132–138.
- [21] M.T. Bore, M.P. Mokhonoana, T.L. Ward, N.J. Coville, A.K. Datye, Microporous Mesoporous Mater. 95 (2006) 118–125.
- [22] B. Lee, Z. Ma, Z. Zhang, C. Park, S. Dai, Microporous Mesoporous Mater. 122 (2009) 160–167.
- [23] G. Prieto, J. Zečević, H. Friedrich, K.P. De Jong, P.E. De Jongh, Nat. Mater. 12 (2013) 34–39.
- [24] B. Liu, T. Jiang, H. Zheng, S. Dissanayke, W. Song, A. Federico, S.L. Suib, J. He, Nanoscale 9 (2017) 6380–6390.
- [25] P.M. Arnal, M. Comotti, F. Schüth, Angew. Chemie 118 (2006) 8404–8407.
- [26] A.B. Laursen, K.T. Højholt, L.F. Lundegaard, S.B. Simonsen, S. Helveg, F. Schüth, M. Paul, J.D. Grunwaldt, S. Kegnœs, C.H. Christensen, K. Egeblad, Angew. Chemie Int. Ed. 49 (2010) 3504–3507.
- [27] G.C. Fryburg, H.M. Petrus, J. Electrochem. Soc. 108 (1961) 496.
- [28] M.T. Bore, T.L. Ward, A. Fukuoka, A.K. Datye, Catal. Letters 98 (2004) 167–172.

- [29] P.S. Dhillon, M.P. Harold, D. Wang, A. Kumar, S. Joshi, Catal. Today 320 (2019) 20–29.
- [30] S.Y. Joshi, Y. Ren, M.P. Harold, V. Balakotaiah, Appl. Catal. B Environ. 102 (2011) 484–495.